ELSEVIER

Polymer 40 (1999) 6451–6463

polymer

Miscible binary blends of poly(ethylene oxide) and an amorphous aromatic polyamide (Aramide 34I): crystallization, melting behavior and semi-crystalline morphology

G. Dreezen[a], M.H.J. Koch[b], H. Reynaers[a], G. Groeninckx[a,*]

[a]*Catholic University of Leuven (KULeuven), Department of Chemistry, Laboratory of Macromolecular Structural Chemistry, Celestijnenlaan 200F, B-3001 Heverlee, Belgium*

[b]*European Molecular Biology Laboratory, Hamburg Outstation EMBL, c/o DESY, Notkestrasse 85, D-22603 Hamburg, Germany*

Received 24 August 1998; received in revised form 3 December 1998; accepted 3 December 1998

Abstract

The crystallizable component poly(ethylene oxide) (PEO) displays liquid–liquid phase separation in blends with the rigid amorphous aromatic polyamide, Aramide 34I. The crystallization, melting behavior and the semi-crystalline morphology after crystallization from the miscible state, are investigated. It is found that the amorphous component, Aramide 34I, has a pronounced effect on the crystallization behavior of PEO; PEO can only be crystallized up to 35 wt.% of Aramide 34I. A complex melting behavior of PEO with secondary crystallization and recrystallization, in which the amorphous component segregates interlamellarly during crystallization, is described. A lamellar insertion model is proposed for the location of the secondary lamellae.

Keywords: Miscible PEO/Aramide 34I blends; Crystallization and melting behavior; Semi-crystalline morphology

1. Introduction

The combination of different thermodynamic phase transitions such as liquid–liquid phase separation, remixing or crystallization in binary polymer blends often result in complex phase diagrams. During morphology formation, these processes can compete kinetically in some temperature and concentration ranges, resulting in a variety of specific blend morphologies with different physical properties. The present project attempts to investigate the morphology formation in binary blends of a crystallizable and an amorphous component, with a lower critical solution temperature (LCST). Until now only a few binary blend systems displaying crystallization and LCST-type liquid–liquid demixing have been studied [1–10].

Blends of the crystallizable component poly(ethylene oxide) (PEO) and the amorphous aromatic component poly(3,4′-diphenylene ether isophtaloyl amide) (Aramide 34I) are miscible over the whole composition range below 120°C. Above this temperature, the system displays LCST-demixing. Blends of PEO and poly(ether sulphone) [11,12] display a similar phase behavior. A thorough understanding of the morphology formation in such blends obtained by crystallization after demixing or remixing in competition with crystallization requires a detailed study of their crystallization kinetics, melting behavior and morphology.

The crystallization behavior of PEO in miscible blends with amorphous components such as PMMA, PEMA, EVAc and PVPh has been extensively studied [13–21]. Alfonso and Russell [22] investigated the PEO/PMMA blend system and developed a modified equation describing the spherulite growth rate in blends of a crystallizable and an amorphous component. Several authors [23–25] investigated the final semi-crystalline morphology and melting behavior after crystallization in miscible blends with PEO. Recently, Talibuddin et al. [26] published the results of an investigation on the segregation behavior of the amorphous component in blends with PEO. To our knowledge, the present article is the first study on the crystallization kinetics, morphology and melting behavior of miscible PEO/Aramide 34I blends. The influence of Aramide 34I on the crystallization kinetics of PEO will be discussed in detail and related to the supramolecular morphology. The melting behavior is profoundly investigated and interpreted from the crystallization kinetics. Based on these discussions, a model for the semi-crystalline morphology in PEO/Aramide 34I blends will be proposed.

* Corresponding author. Tel.: + 32-16-32-74-40; fax: + 32-16-32-74-90.

0032-3861/99/$ - see front matter
PII: S0032-3861(98)00849-0

2. Experimental

2.1. Materials and blend preparation

PEO with a viscosity average molecular weight of 20 000 and a polydispersity of 1.2, obtained from FLUKA Chemie AG, was blended with a laboratory synthesized [27] poly(3,4′-diphenylene ether isophtaloyl amide) (Aramide 34I) with a weight average molecular weight of 36 000 and a polydispersity of 2.04 in wt/wt compositions of 95/5, 90/10, 85/15, 80/20, 77/23, 75/25, 65/35 and 50/50. Blends were prepared by solution casting from 10% solutions in pyridine; after evaporation of the solvent, they were dried under vacuum at 80°C for 48 h to remove the residual solvent. Before every experiment the blend samples were dried at 60°C under vacuum for 12 h to remove all absorbed water. The glass-transition temperature of PEO is −60°C and that of the amorphous component Aramide 34I is 224°C.

2.2. Optical microscopy

Cloud points were detected from the light transmitted by thin samples between glass-slides under an OLYMPUS optical microscope coupled with a computer controlled CCD-camera. The same device was used to measure the spherulite growth rates of PEO in the blends. At different times during the growth process, images of the sample obtained with the polarizers under 45° were stored. The spherulite growth rate was calculated from the increase of the spherulite radius with time for all blends that crystallized over a reasonable time (5 h), at temperatures between 15°C and 55°C. The resulting supramolecular morphology was investigated under the same microscope with crossed polarizers.

2.3. Differential scanning calorimetry

Differential scanning calorimetry (DSC)-measurements were performed on a Perkin–Elmer DSC-7 using approximately 5 mg of sample. After isothermal crystallization, the samples were heated at a rate of 10°C/min to determine the melting behavior. Dynamic crystallization experiments were started from 100°C at a cooling rate of −10°/min. DSC-measurements performed at different heating rates were corrected for the temperature shift of the indium calibration sample and normalized to a heating rate of 1°/min. The crystallinity was determined from the DSC melting curves according to the method of Mathot et al. [28]. The advantage of this method is that the crystallinity does not depend on the definition of an arbitrary baseline under the melting peak, but yields an analyst-independent determination of the transition enthalpy via an area determination with a baseline extrapolated from the melt. The crystallinity as function of temperature during cooling or heating is determined from:

$$X_c(T) = \frac{[A_2 - A_1]_T}{\Delta h(T)} \tag{1}$$

where $[A_2 - A_1]_T$ is the transition enthalpy. The temperature-dependent enthalpy function $\Delta h(T) = h_a(T) - h_c(T)$ is available from the ATHAS databank [29–32] for several types of semi-crystalline polymers.

2.4. Real time small angle X-ray scattering

Time resolved synchrotron radiation experiments were carried out on the double focussing camera X33 [33] of the EMBL in HASYLAB on the storage ring DORIS of the Deutsches Elektronen Synchrotron (DESY) at Hamburg using a wavelength λ of 1.5 Å. Samples with a thickness of 1 mm were sealed between thin aluminum foils. SAXS and WAXD patterns were simultaneously collected using gas proportional detectors [34] every 12 s during isothermal or heating experiments at a heating rate of 10°C/min (i.e. 1 pattern/2°C). A temperature program similar to that used for DSC-measurements was maintained using a Mettler FP82 hot stage mounted in the X-ray beam path.

The SAXS-data were corrected for background scattering by the subtraction of an amorphous sample in the molten state and Lorentz corrections were applied. The long period, L_{lor}, was obtained from the maximum in the Lorentz corrected intensity profiles. The lamellar and amorphous layer thickness (l_c and l_a), and another value for the long period ($L_{c.f}$) were obtained from the one-dimensional correlation function [35] given by:

$$\gamma_1(r) = \frac{\int_0^\infty I(s)\, s^2 \cos(2\pi r s)\, \mathrm{d}r}{\int_0^\infty I(s)\, s^2\, \mathrm{d}s} \tag{2}$$

where $s = (2 \sin \theta)/\lambda$, with 2θ as the diffraction angle and r the dimension in real space.

Prior to Fourier transformation, the data were extrapolated to high angles using Porod's law:

$$Is^4 = K_p \exp(-4\pi^2\sigma^2 s^2) \tag{3}$$

where K_p is the Porod constant and σ describes the electron density profile at the interface between the amorphous and crystalline sections.

The data were extrapolated to zero s-value assuming a constant I versus s profile. The normalization of the correlation function was based on an ideal lamellar crystalline/amorphous morphology which yields a value for the invariant $\gamma_1(0) < 1$ [35]. The degree of crystallinity φ within the lamellar stacks can be determined from the quadratic expression:

$$\varphi(1 - \varphi)L_{c.f.} = A \tag{4}$$

where A is the first intercept of the correlation function with the x-axis or from the minimum of the correlation

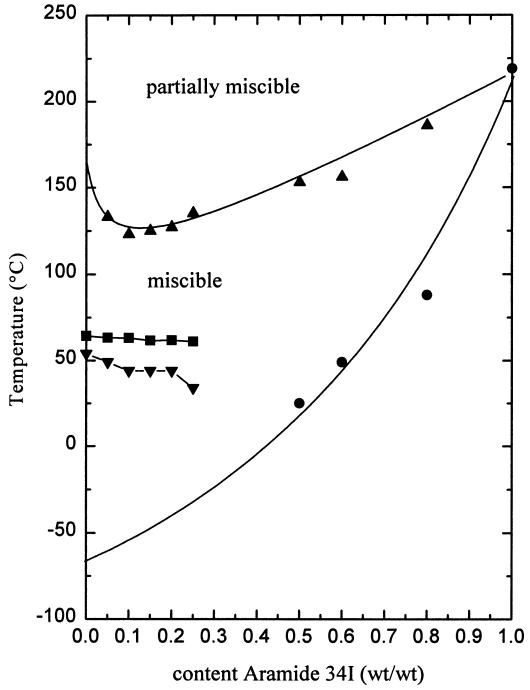

Fig. 1. Phase diagram of PEO/Aramide 34I blends (▲ cloud point, ■ melting point, ▼ upper isothermal crystallization temperature, ● glass-transition temperature).

function:

$$-\frac{1-\varphi}{\varphi} = \gamma_1(r)_{\min} \tag{5}$$

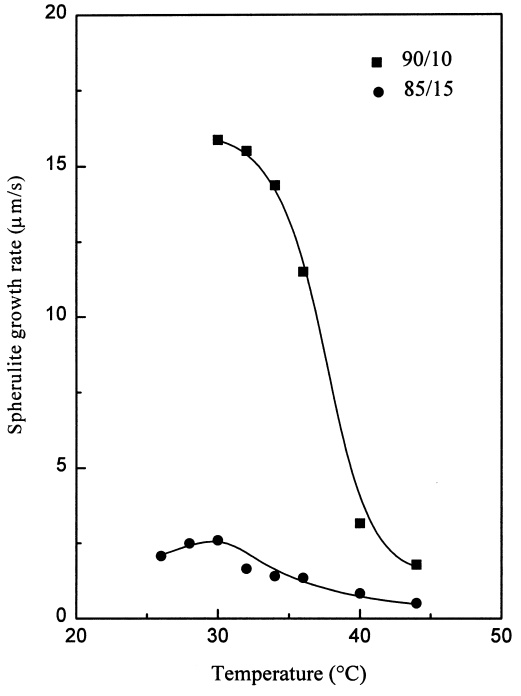

Fig. 2. Spherulite growth rate versus temperature of a 90/10 and 85/15 PEO/Aramide 34I blend.

The latter equation is only valid if there is a flat minimum in the correlation function. Finally, the amorphous layer thickness l_a can be determined from the intersection of the horizontal baseline drawn at $-(1-\varphi)/\varphi$ with the tangent of the self-correlation part of $\gamma_1(r)$ if the crystallinity is above 50% [35]. The crystalline layer thickness is derived from:

$$L_{c.f.} = l_c + l_a \tag{6}$$

The thickness of the interface cannot be determined using the normalization procedure described previously, which is based on an ideal two-phase system.

3. Results and discussion

3.1. Phase diagram of PEO/Aramide 34I blends

The phase diagram of PEO and Aramide 34I is presented in Fig. 1; the lower critical solution temperature is observed for 90/10 PEO/Aramide 34I blend at 120°C. The cloud point curve is flat and asymmetric. The crystallization curve (T_c) indicates the upper temperature limit where blends crystallize within 4 h. Dynamic crystallization of PEO in blends with Aramide 34I at a cooling rate of -10°/min is possible up to 20 wt.% amorphous Aramide 34I. Isothermal crystallization for long periods (450 h) revealed that PEO can crystallize in blends up to 35 wt.% Aramide 34I. The glass-transition temperature T_g of the blends, as calculated from the Fox-equation [36], changes rapidly with increasing content of Aramide 34I, which has a high T_g. All experiments considered later were started from a temperature in the one-phase miscible region below the cloud point curve.

3.2. Crystallization behavior of PEO in miscible blends with Aramide 34I

Crystallization kinetics in bulk semi-crystalline homopolymers have been described in the past using a modified version [37,38] of the nucleation theory of Turnbull and Fisher [39,40]. In this treatment, the spherulite growth rate G depends on the energy necessary to transport chain segments across the liquid–solid interface (ΔE) and the energy required to form a critical nucleus (ΔF^*) on the lamellar surface (secondary nucleation):

$$G = G_0 \exp\left[\frac{-\Delta E}{RT_c}\right]\exp\left[\frac{-\Delta F^*}{k_B T_c}\right] \tag{7}$$

where G_0 is the growth rate constant, T_c the crystallization temperature, R, the gas constant and k_B, the Boltzmann constant. The growth rate of the semi-crystalline component (G_{bl}) in miscible blends with an amorphous component as derived from the phenomenological description of Alfonso and Russell [22], is given by:

$$G_{bl} = \frac{\varphi_2 k_1 k_2}{k_1 + k_2}\exp\left[\frac{-\Delta F_{bl}^*}{k_B T_c}\right] \tag{8}$$

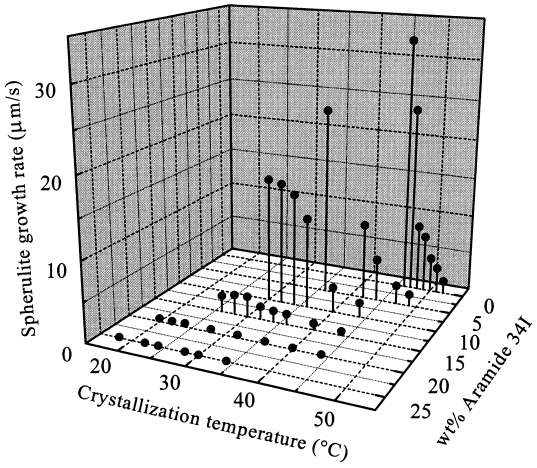

Fig. 3. Spherulite growth rate as a function of temperature and content of amorphous component Aramide 34I.

where φ_2 is the volume fraction of the amorphous component, k_1 represents the transport rate of the crystalline segments to the liquid–solid interphase, k_2 is the diffusion rate of the amorphous component from the crystalline growth front. This description takes into account the specific interactions between the blend components, the diffusion of the amorphous component, the blend T_g and the dilution of the crystallizable component.

Typical spherulite growth rate curves determined by optical microscopy of 90/10 and 85/15 PEO/Aramide 34I blends are given in Fig. 2. The spherulite growth rate of PEO in the 90/10 blend increases with decreasing crystallization temperature; at lower crystallization temperatures, the nucleation density is high so that the spherulites rapidly impinge and/or the crystallization starts before the isothermal crystallization temperature is reached. The spherulite growth rate curve of the 85/15 PEO/Aramide 34I blend exhibits a clear maximum, indicating a change from the nucleation controlled crystallization at low degrees of undercooling to diffusion controlled crystallization at high degrees of undercooling. The change of the spherulite growth rate as a function of the amount of amorphous component Aramide 34I and the crystallization temperature is shown in Fig. 3. The spherulite growth rate at the highest and the lowest measured isothermal crystallization temperature is indicated in Table 1. The growth rate decreases strongly with increasing Aramide 34I content; for a blend with 30% Aramide 34I, no crystallization of PEO occurs within a measurement time of 5 h. Further, a higher degree of undercooling is required to crystallize PEO with increasing amount of Aramide 34I. While pure PEO crystallizes below a temperature of 56°C, it displays a 75/25 PEO/Aramide 34I blend crystallization below 30°C.

Several factors must be considered to explain the pronounced change in the crystallization behavior of PEO in the presence of Aramide 34I. First, the decrease of the spherulite growth rate of PEO in PEO/Aramide 34I blends is more pronounced and crystallization only occurs at lower temperatures compared to the crystallization of PEO in miscible blends with the amorphous components PMMA, PEMA, PVAc and EVAc [13–20]. The latter polymers have a lower T_g than Aramide 34I, and despite differences in specific interactions between PEO and the various amorphous components, it is clear that the relatively high T_g of the PEO/Aramide blends has a large influence on the crystallization kinetics. Secondly, it has been emphasized [41] that in some cases crystallization in polymer blends can be kinetically prevented although it is thermodynamically possible.

The increasing T_g of PEO/Aramide blends is accompanied by a strong decrease of the mobility of the PEO chains. This is the determining factor for the low spherulite growth rate in blends with a small amount of Aramide 34I, as well as in the prevention of crystallization in blends with a higher amount (>40 wt.%) of Aramide 34I. The specific interactions, diffusion of the amorphous component and dilution effect, although important, play a secondary role in the described effects.

From the spherulite growth rate data, the nucleation

Table 1
Spherulite growth rate at the upper and lower isothermal crystallization temperature, nucleation regime and product of the lateral and surface lamellar free energy $\sigma\sigma_e$ of PEO/Aramide 34I blends

PEO/Aramide composition	Temperature (°C)	Spherulite growth rate (μm/s)	Nucleation regime	$\sigma\sigma_e$ (10^7 J/cm^2)^2
100/0	54	0.39	II	611
	44	33.59		
95/5	49	1.07	II	656
	36	23.97		
90/10	44	1.78	II	724
	30	15.87		
85/15	44	0.5	III	877
	26	2.07		
80/20	44	0.13	III	903
	20	0.39		
75/25	34	0.059	III	1247
	19	0.065		

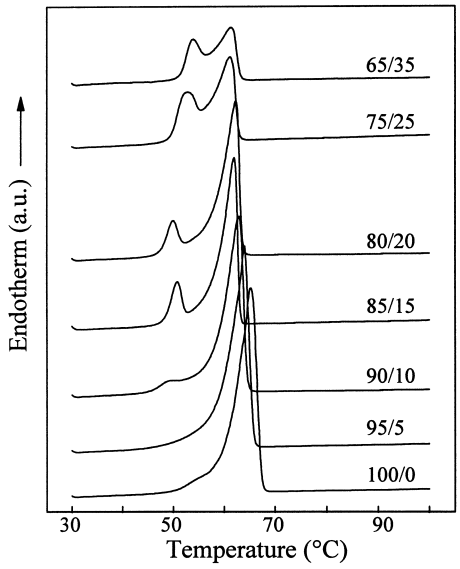

Fig. 4. DSC-heating curves measured at a rate of 10°/min of PEO/Aramide blends crystallized at 28°C for 450 h.

regime and the fold surface free energy can be evaluated. Eq. (7) [38] can be rewritten in terms of an activation energy U^* required for transport of chain segments across the liquid–solid interface and a nucleation term K_g describing the secondary nucleation process:

$$\ln G + \frac{U^*}{R(T_c - T_\infty)} = \ln G_0 - K_g\left(\frac{1}{fT_c\Delta T}\right) \quad (9)$$

where $U^* = 4120$ cal/mol [38], $T_\infty = T_g - 51.3$, $\Delta T = T_m^0 - T_c$, $f = 2T_c/(T_c + T_m^0)$, K_g is $2jb\sigma\sigma_e T_m^0/f\Delta h_f k_B$ with $\sigma\sigma_e$ the product of the lateral and fold surface free energy, Δh_f is the heat of fusion per mole monomer (i.e. 196.4 J/g [29–32]), b is the thickness of a monomolecular layer (4.65 Å) and T_m^0 is the equilibrium melting temperature of PEO: (73°C), j is a constant 1 for nucleation regime I, 2 for nucleation regime III.

A plot of the left-hand side of Eq. (9) versus $1/fT_c\Delta T$ allows us to calculate K_g from the slope. Interpretation of the crystallization process in terms of a nucleation regime (I, II or III), as described by Lauritzen [38], is possible from K_g. One defines a parameter Z as:

$$Z = 10^3\left(\frac{l_c}{2b}\right)\exp\left(\frac{-X}{T_c\Delta T}\right) \quad (10)$$

where l_c is the lamellar thickness. When $X = K_g$ and $Z \leq 0.01$, crystallization occurs according to regime I in which a secondary nucleus formed on the crystallizing lamellar surface rapidly completes the layer. When $X = 2K_g$ and $Z \geq 1$, crystallization occurs according to regime III, where many secondary surface nuclei form before the lamellar layer is completed. In all other cases the intermediate regime II is followed. The lamellar thickness was estimated from Spegt [42] and gave a satisfactory agreement with the few data points in our study. These results are summarized in Table 1.

Pure PEO and the 95/5 and 90/10 PEO/Aramide 34I blends crystallize according to the intermediate crystallization regime II in which formation of secondary nuclei competes with the completion of the lamellar surface. From 15% amorphous component onwards, the crystallization process is controlled by regime III where nuclei are formed in large numbers on the lamellar surface substrate and spread slowly. The change in nucleation regime can be inferred from experimental observations: first, the decrease of the crystallization temperature with increasing amount of amorphous component results in an increase of the surface nucleation rate and a decrease of the chain mobility by which regime III is favored. Secondly, although the 90/10 and 85/15 PEO/Aramide 34I blends crystallize in the same temperature range between 25°C and 45°C, they display a different regime of nucleation (II and III). In blends with a higher amount of Aramide 34I, the mobility of PEO is lower, which retards the completion of the lamellar surface. In combination with a nearly unchanged rate of formation of secondary nuclei this might result in a change from regime of nucleation II to III.

The product of the lateral and fold surface free energy $\sigma\sigma_e$ of the PEO lamellar crystals is obtained from the nucleation term K_g. The results presented in Table 1 show that $\sigma\sigma_e$ increases with higher amount of Aramide 34I in the blend. One can assume that the lateral surface free energy σ is independent of the amount of amorphous component and remains a constant [20,38]. The increase of the fold surface free energy σ_e can be as a result of the decreased mobility of PEO during crystallization in blends with a large amount of Aramide 34I, which results in the formation of less coarser lamellar folds. For PEO/PMMA blends, Martuscelli et al. [20] reported a monotonic decrease of $\sigma\sigma_e$ and proposed that larger lamellar loops form as a result of the entanglements with interlamellar segregated PMMA molecules. The decrease of the spherulite growth rate for this blend system is, however, much smaller than for the PEO/Aramide blends. However, the increase of $\sigma\sigma_e$ might also be attributed to the variation of the equilibrium melting temperature T_m^0 with changing blend composition. A correct value of T_m^0 for PEO/Aramide blends could not be determined from Hoffman–Weeks plots as a result of the presence of recystallization. T_m^0 can be estimated assuming that $\sigma\sigma_e$ remains constant with changing blend composition [43]. For 75/25 PEO/Aramide blends this results in a decrease of T_m^0 of 16°C. This decrease in miscible blends of PEO with an amorphous component is too large and we conclude that the observed increase of $\sigma\sigma_e$ can not only be attributed to a decrease of the equilibrium melting temperature.

3.3. Melting behavior of PEO/Aramide blends

The DSC melting behavior of miscible PEO/Aramide 34I blends after isothermal crystallization was investigated.

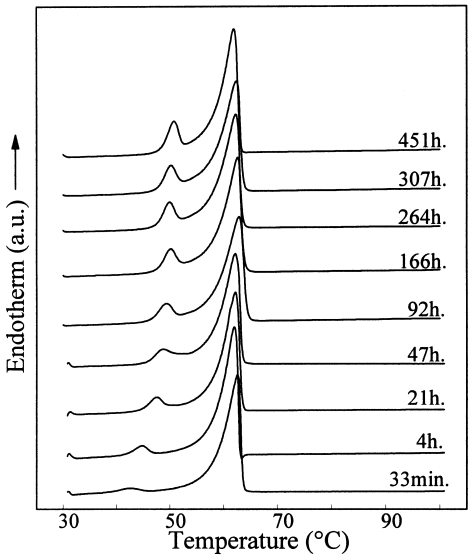

Fig. 5. DSC-heating curves of 85/15 PEO/Aramide blends crystallized at 28°C for different times.

Fig. 4 illustrates the melting thermograms of PEO/Aramide blends with compositions from 100/0 to 65/35, crystallized at 28°C for 450 h. Whereas pure PEO and a 95/5 PEO/Aramide 34I blend display only one melting endotherm (with a small shoulder on the left-hand side), blends with 10% or a higher amount of amorphous component exhibit a second melting endotherm at lower temperatures. There is also a small shift of the melting endotherm at about 65°C to lower temperatures with increasing Aramide 34I content.

The occurrence of multiple melting in a blend of an amorphous and a semi-crystalline component has been attributed by Groeninckx et al. to several processes [44–46], including recrystallization and secondary crystallization. Several experiments were performed to identify the origin of the second melting endotherm. The blends were crystallized for varying times to establish whether or not secondary crystallization occurred. As illustrated in Fig. 5, an 85/15 PEO/Aramide 34I blend was crystallized at 28°C for different times between 33 min (time necessary to complete the primary crystallization) and 450 h. While the primary melting endotherm at 65°C does not change, there is an increase in intensity and a shift from 41°C to 50°C of the second melting endotherm, with increasing crystallization time. These changes can be attributed to secondary crystallization of PEO after the primary crystallization process. The crystallization of some PEO-chains is retarded and they crystallize slowly after the formation of the spherulitic structure. With increasing time, these thin lamellae thicken and melt at higher temperatures. In a 85/15 PEO/Aramide 34I blend, this secondary crystallization process starts during the primary crystallization and continues over a long period of time.

DSC-measurements were carried out at different heating rates between 1 and 40°C/min to detect recrystallization.

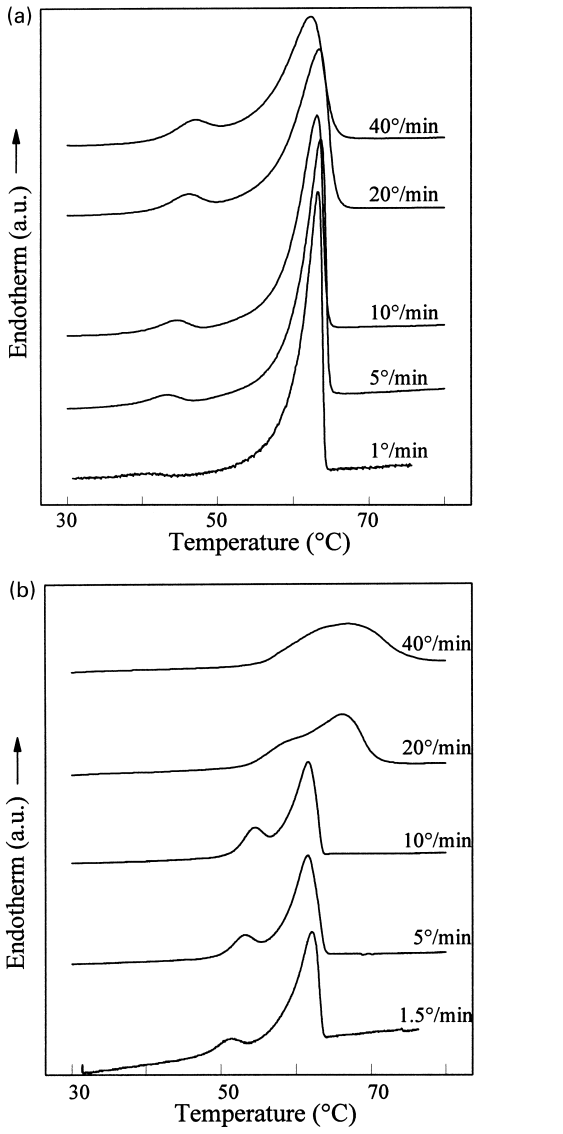

Fig. 6. DSC-curves at different heating rates: (a) for an 80/20 PEO Aramide blend crystallized at 28°C for 60 min; (b) for a 65/35 PEO/Aramide blend crystallized at 28°C for 450 h.

The thermograms of an 80/20 PEO/Aramide blend, crystallized at 28°C for 60 min, are shown in Fig. 6(a). The lower endotherm shifts to higher temperatures and becomes more pronounced at higher heating rates, while the higher endotherm at 65°C decreases and shifts slightly to lower temperatures. Apparently, both secondary crystallization and recrystallization occur in an 80/20 PEO/Aramide blend. After primary crystallization of PEO within a short time interval (30 min), a secondary crystallization process starts during which thin lamellae, melting at lower temperatures, are formed. During heating at low heating rates these lamellae melt and recrystallize, resulting in the lower melting endotherm that is shifted to lower temperatures, as illustrated in Fig. 7(a). The recrystallized lamellae melt at slightly higher temperature than the thick primary lamellae with a shift to higher temperature and an increase in

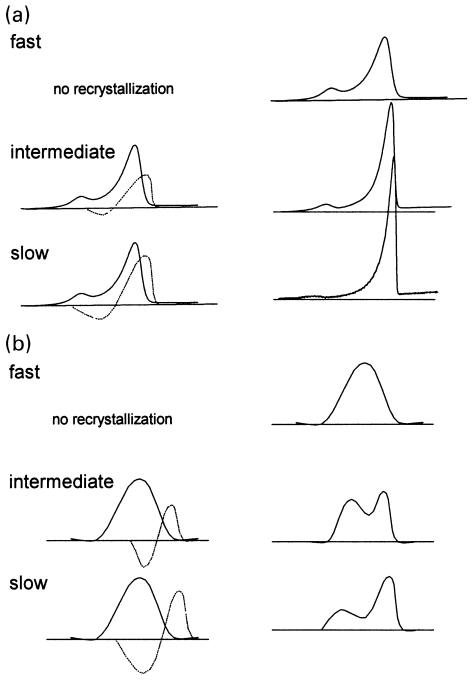

Fig. 7. Schematic representation of the melting mechanism proposed to account for the heating rate dependence of recrystallizing blends. The left side of the figure shows the melting of the original crystals (full line) and the recrystallization, remelting phenomenon (dashed line), the right side shows the resulting experimentally observed thermogram: (a) for an 80/20 PEO/Aramide blend; (b) for a 65/35 PEO/Aramide blend at fast, intermediate and slow heating rates.

intensity of the higher melting endotherm as compared to DSC-curves at a heating rate of 40°C, where no or only little recrystallization occurs.

A 65/35 PEO/Aramide blend requires longer crystallization time than the 80/20 PEO/Aramide blend. DSC melting curves at different heating rates of a 65/35 PEO/Aramide blend after crystallization at 28°C for 450 h are presented in Fig. 6(b). The lower melting endotherm shifts towards the higher melting endotherm and becomes more pronounced at higher heating rates. At a heating rate of 40°C/min, one broad melting endotherm is present. For the 65/35 PEO/Aramide blend it can be concluded that during the slow isothermal crystallization process only one type of lamellae is formed with a broad distribution. The interlamellar amorphous phase contains a higher amount of Aramide inhibiting further secondary crystallization process of PEO, in contrast to the 80/20 PEO/Aramide blends. At low heating rates lamellae melt, recrystallize and remelt again at higher temperatures. The double melting endotherm is the superposition of these phenomena, a model description is presented in Fig. 7(b). With increasing heating rate, a smaller fraction of the lamellae is able to recrystallize. At high heating rates none or only a small amount of lamellae recrystallizes leading to a broad melting endotherm.

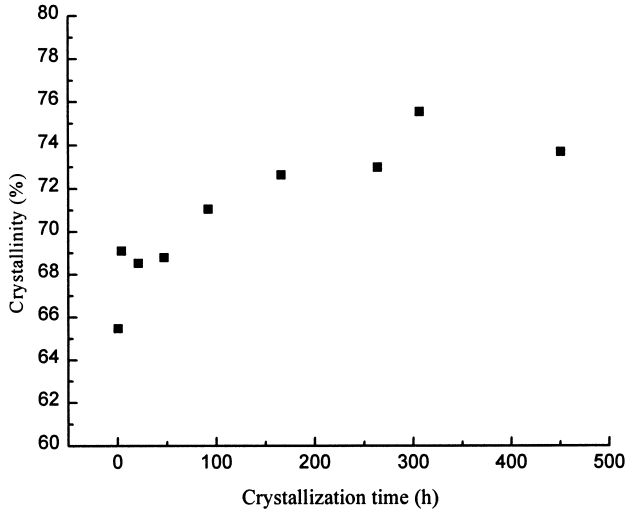

Fig. 8. Degree of crystallinity from DSC-heating curves as a function of crystallization time of PEO in 85/15 PEO/Aramide blends crystallized at 28°C.

The influence of the secondary crystallization process on the degree of crystallinity is illustrated in Fig. 8 where the crystallinity of PEO as a function of the crystallization time in the 85/15 PEO/Aramide blend is presented. With increasing time, the degree of crystallinity increases from 65% to 75%. The degree of crystallinity for different blends crystallized at 28°C for 450 h is shown in Fig. 9. The crystallinity of PEO in the blends decreases from 96% for pure PEO to 56% for a 65/35 PEO/Aramide blend. Besides the strong decrease of the spherulite growth rate of PEO in blends with Aramide 34I, the lower degree of crystallinity of PEO clearly indicates the pronounced influence of the amorphous aromatic component on the crystallization behavior of PEO. The high crystallinity value for pure PEO results from the evaluation method, which relies on a temperature dependent Δh-function. Using the conventional method, a value of 85% is obtained in agreement with previous reports [20,25] by dividing the experimental melting enthalpy by the heat of fusion (196.4 J/g) at T_m^0 of 100% crystalline PEO.

3.4. Supramolecular structure and semi-crystalline morphology of PEO/Aramide blends

The supramolecular structure of pure PEO consists of different types depending on the molecular weight and the crystallization temperature. Mandelkern et al. [47] compiled a morphological map for PEO in which three different supramolecular structures are present: a spherulitic, a hedritic and an intermediate spherulitic-hedritic structure. In the present paper, the supramolecular structure of PEO and the PEO/Aramide 34I blends was investigated by polarized light microscopy, as illustrated in Fig. 10. Pure PEO displays a non-structured birefringence structure. Blending of PEO with Aramide 34I results in the formation of well-formed Maltese crosses above 15% Aramide 34I.

According to Mandelkern's morphological map, PEO with a molecular weight of 20 000, as used here, crystallizes in an intermediate spherulitic-hedritic structure in

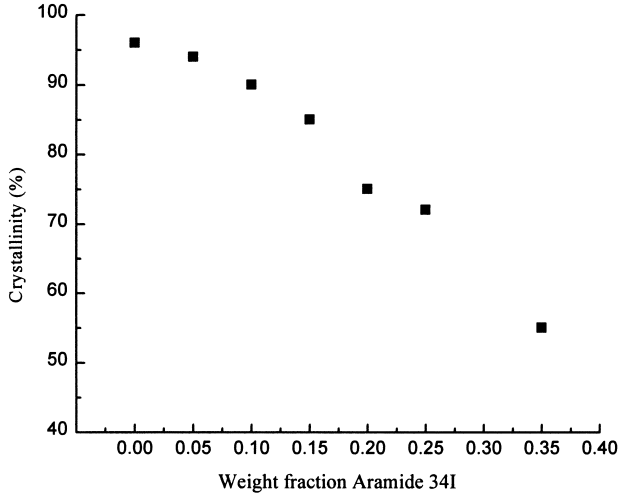

Fig. 9. Degree of crystallinity from DSC heating curves as a function of weight fraction Aramide 34I of PEO in PEO/Aramide 34I blends crystallized for 450 h at 28°C.

agreement with the pattern shown in Fig. 10(a). The Maltese-crosses of the 85/15 blend indicate that the supramolecular structure of PEO in blends containing more than 15% Aramide 34I is completely spherulitic. A similar change in the supramolecular structure of PEO in blends with PVAc [16] was also reported. The occurrence of intermediate spherulitic-hedritic and spherulitic structures suggests an explanation for the change in supramolecular structure of PEO in blends with Aramide 34I. Whereas hedrites are more or less layered lamellar structures grown from a central screw dislocation, spherulites are lamellar structures that grow in three dimensions. In the presence of Aramide 34I a much higher degree of undercooling is necessary to crystallize PEO in the blends, as shown in the study of the spherulite growth rate. At these lower temperatures, the secondary nucleation rate is larger and the lateral growth rate decreases as already expressed by the change of the nucleation regime from II to III between a 90/10 and an 85/15 PEO/Aramide 34I blend. This results in a three-dimensional growth and the formation of a spherulitic supramolecular structure from 15 wt.% amorphous component upward. A similar relationship between the nucleation regime and the crystalline structure has been reported for linear polyethylene [48]; axialites follow nucleation regime I whereas spherulites follow regime III.

The semi-crystalline morphology is largely determined by the type of segregation (interspherulitic, interfibrillar or interlamellar) of the amorphous component. From Fig. 10 it is clear that for all blends containing up to 25 wt.% amorphous component, volume-filling spherulites are formed indicating intraspherulitic segregation of the Aramide 34I. To find out whether Aramide 34I segregates between lamellae or stacks of lamellae, SAXS-measurements were performed on PEO/Aramide 34I blends isothermally crystallized at 44°C. As a result of the pronounced influence of the amorphous Aramide 34I component on the crystallization behavior, only blends containing up to 15 wt.% Aramide can be crystallized within a reasonable time interval at 44°C. One-dimensional correlation functions were calculated from the experimental SAXS patterns. Morphological parameters, such as the number average long period, crystalline lamellar thickness and amorphous layer thickness are presented in Fig. 11; the long period obtained from Lorentz corrected intensity curves is also added. Both the long period and the amorphous thickness increase with the amount of amorphous component whereas the crystalline lamellar thickness slightly decreases; an effect that can be explained by interlamellar segregation of Aramide 34I during crystallization of PEO.

It has been pointed out [49] that the scale of segregation of the amorphous component during crystallization is related to the ratio between the diffusion rate D of the amorphous component and the growth rate G of the crystalline component. The segregation behavior of several amorphous components with different glass-transition temperatures and types of interactions in PEO blends was recently investigated [26]. It was concluded that although the effect of mobility of the diluent cannot be neglected, it is mainly the growth rate of the PEO crystals that dominates the length scale of segregation. A similar approach can be followed for the PEO/Aramide blends. Aramide 34I has a high T_g and the diffusion rate decreases for higher Aramide 34I content in the blends. Moreover, a strong decrease of the spherulite growth rate of PEO with increasing content of the amorphous component was observed and attributed to the decreased mobility of PEO on adding amorphous component. From our SAXS-experiments it can be concluded that in blends containing up to 23 wt.% Aramide, the amorphous component segregates interlamellarly. The strong decrease in the growth rate of the crystals is thus accompanied by a low diffusion rate of the amorphous component in PEO/Aramide blend, and consequently both factors are important in the segregation behavior.

Two morphological models can be proposed for the secondary crystallization: the dual lamellar stack model [50] with the thick primary and thin secondary lamellae in separate stacks, and the lamellar insertion model [51,52] with the thin lamellae inserted between the thick ones in the same stack. Time resolved small angle X-ray scattering experiments during isothermal crystallization and melting of the PEO/Aramide blends were performed to distinguish between these possible models.

The Lorentz-corrected SAXS-patterns of an 80/20 blend during: (a) isothermal crystallization at 28°C for 60 min, (b) heating of this sample at a rate of 10°/min from 28°C to 80°C, and (c) heating at a rate of 10°/min after crystallization at 28°C for 450 h are shown in Fig. 12. During isothermal crystallization, a single scattering maximum corresponding to a long period $L_{lor} = 160$ Å appears. No additional maxima appear during the isothermal crystallization process within 60 min. The SAXS-curve of the annealed sample at 30°C displays a similar profile. From

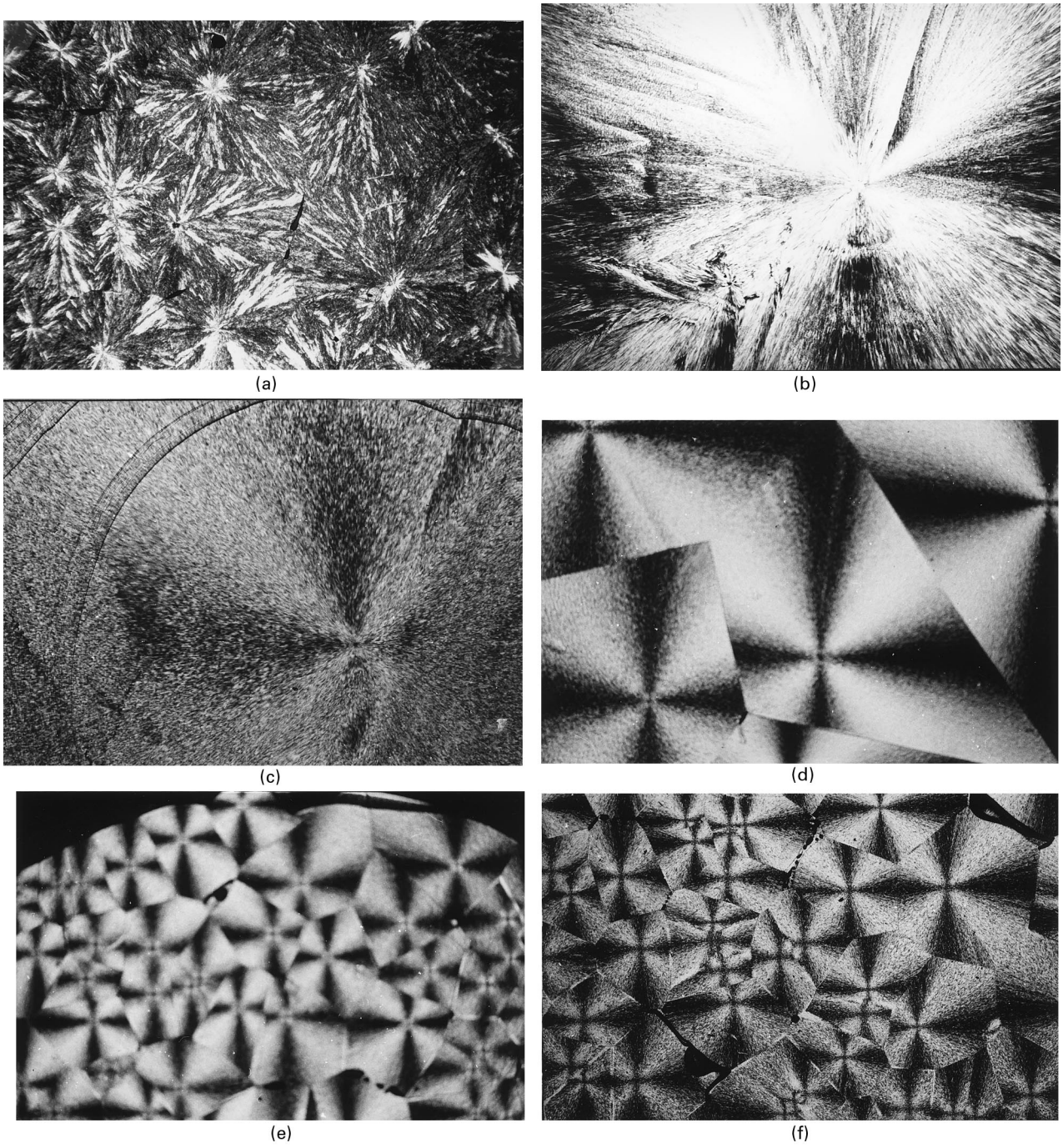

Fig. 10. Optical micrographs of PEO/Aramide blends: (a) 100/0 $T_c = 47°C$, magn. 5×; (b) 95/5 $T_c = 42°C$, magn. 5×; (c) 90/10 $T_c = 44°C$, magn. 10×; (d) 85/15 $T_c = 32°C$, magn. 10×; (e) 80/20 $T_c = 28°C$, magn. 10×; (f) 75/25 $T_c = 28°C$, magn. 10×.

these observations it can be concluded that secondary crystallization occurs according to the lamellar insertion model where the secondary thin lamellae are formed between the thicker primary lamellae. For the dual lamellar stack model, the secondary lamellar stacks would be expected to give a scattering maximum corresponding to a different long period than the primary lamellar stacks, this is however not observed.

Correlation functions calculated from the spectra obtained during heating of the 80/20 PEO/Aramide blend crystallized at 28°C for 60 min are presented in Fig. 13, and the corresponding DSC heating curves and morphological parameters are given in Fig. 14. No morphological parameters are shown for temperatures above 55°C; the crystallinity decreases below 60% and the correlation function analysis becomes unreliable. The secondary crystallization process results in a shift and an increase in intensity of the first melting endotherm. The long period of the annealed

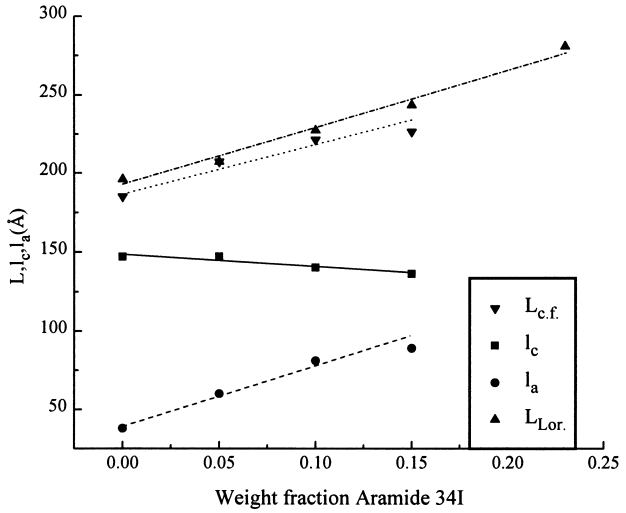

Fig. 11. Morphological parameters of PEO/Aramide blends crystalized isothermally at 44°C: ▲ long period from Lorentz corrected pattern L_{lor}; ▼ long period from correlation function $L_{c.f.}$; ■ crystalline lamellar thickness l_c; ● amorphous layer thickness l_a.

sample is initially 20 Å larger than that of the non-annealed sample. During heating, the long period of the non-annealed sample increases and reaches the same value as that of the annealed sample at 48°C. Above this temperature, the annealed sample starts to melt and its long period also increases. The crystalline lamellar thickness of the annealed sample is larger than that of the non-annealed sample, whereas the amorphous layer thickness is approximately the same.

Several aspects have to be considered in the interpretation of these results. Aramide 34I segregates interlamellarly during crystallization of PEO in PEO/Aramide 34I blends. This results in the formation of a miscible amorphous PEO/Aramide phase between the crystalline lamellae containing an increased amount of amorphous aromatic component. In this phase the mobility decreases and the crystallization of PEO becomes difficult, if at all possible. It was shown that a 65/35 PEO/Aramide blend crystallizes very slowly and a 50/50 PEO/Aramide is completely amorphous (see Fig. 1 and discussion of the phase diagram). One can assume that a decreasing concentration gradient of PEO chains extends from the crystalline lamellae towards the amorphous PEO/Aramide phase between these lamellae. Consequently, during annealing most of the secondary lamellae are formed and they thicken close to the primary ones, whereas in the center between the primary lamellae at most a few secondary lamellae can be formed. A possible explanation for the increased long period and crystal thickness after annealing is that some of the secondary lamellae initially contribute individually to the average long period and lamellar thickness. During annealing these secondary lamellae grow and thicken close to the primary ones, forming finally a single scattering unit resulting in a larger average long period and crystal thickness.

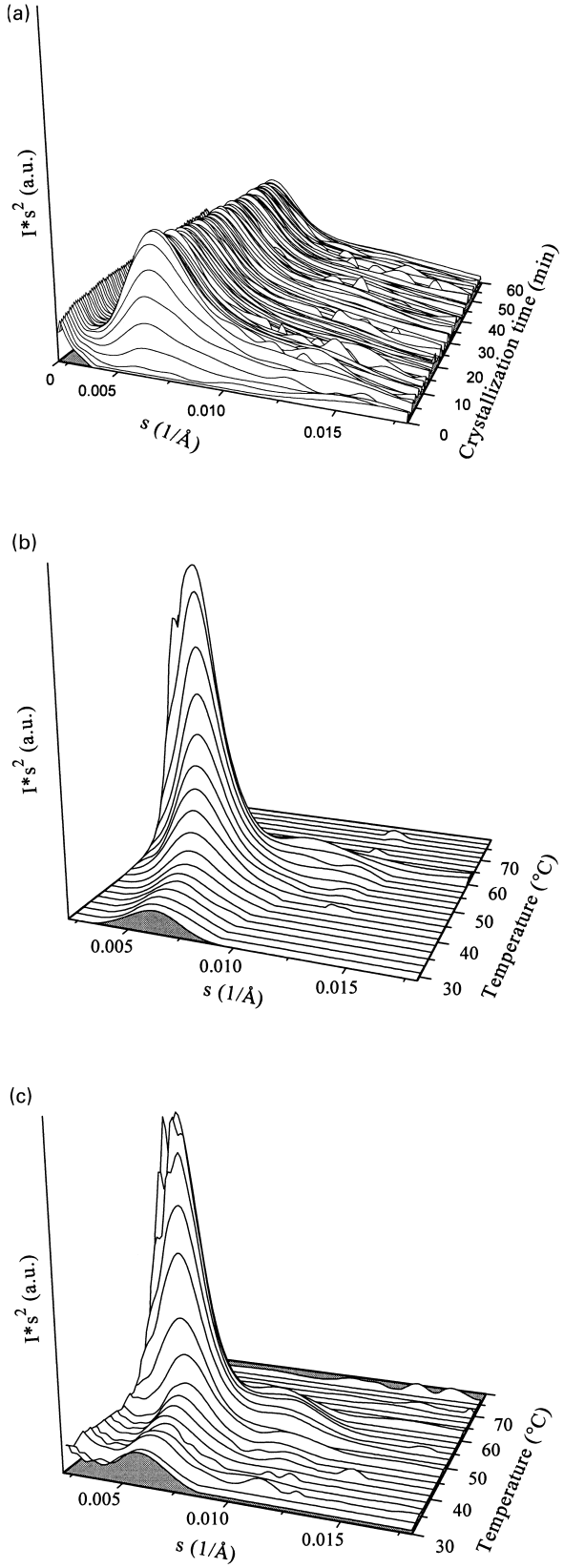

Fig. 12. Lorentz corrected SAXS-patterns of an 80/20 PEO/Aramide blend: (a) during isothermal crystallization at 28°C for 60 min; (b) heating at 10°/min after 60 min at 28°C, and (c) heating at 10°/min after 450 h at 28°C. The spikes in the curves are an artefact of the spline smoothing.

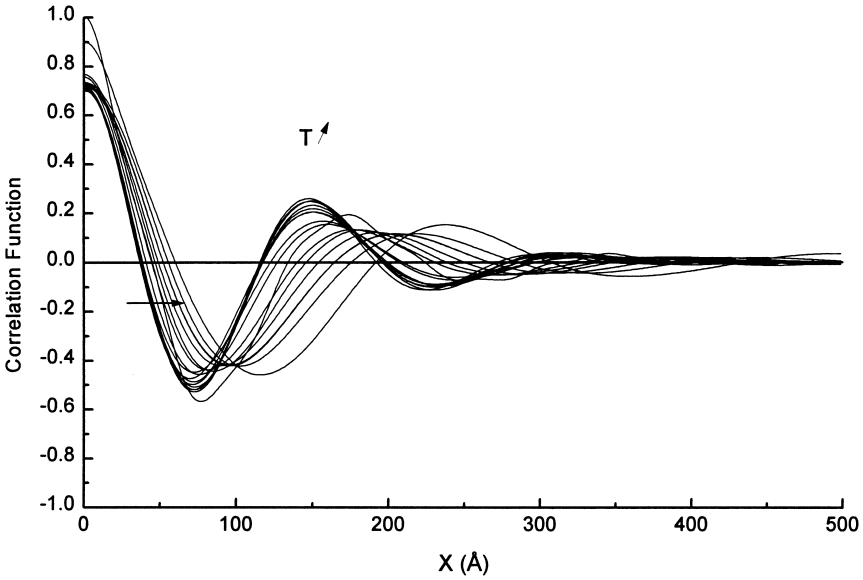

Fig. 13. Correlation functions during heating at 10°/min from 28 to 62°C of an 80/20 PEO/Aramide 34I blend crystallized at 28°C for 60 min.

A model describing the crystallization of PEO/Aramide blends is presented in Fig. 15. In the miscible melt (a) of an 80/20 (or 85/15) PEO/Aramide blend, fast primary crystallization (b) is followed by additional secondary crystallization with secondary lamellae located between the initial primary ones (c). PEO/Aramide blends with higher amount of amorphous component (e.g. 65/35) crystallize more slowly forming only one type of lamellae (d).

4. Conclusions

The crystallization, melting behavior, the supramolecular structure and the semi-crystalline morphology of blends of PEO and Aramide 34I were investigated in the region of miscibility. It was shown that the crystallization behavior of PEO is strongly influenced by the presence of the amorphous Aramide 34I component. PEO can only crystallize in blends containing up to 35 wt.% Aramide. The spherulite

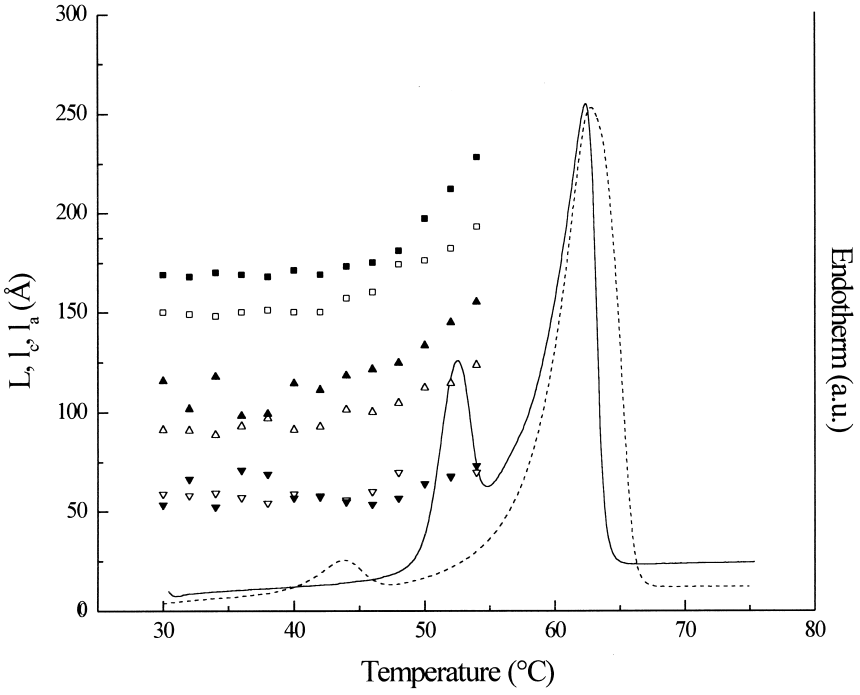

Fig. 14. DSC-melting curves and morphological parameters of PEO/Aramide 80/20 blends crystalized at 28°C: (a) for 60 min (dashed line, open symbols); (b) 18 days (full line and symbols: ■ long period; ▲ lamellar thickness; ▼ amorphous layer thickness).

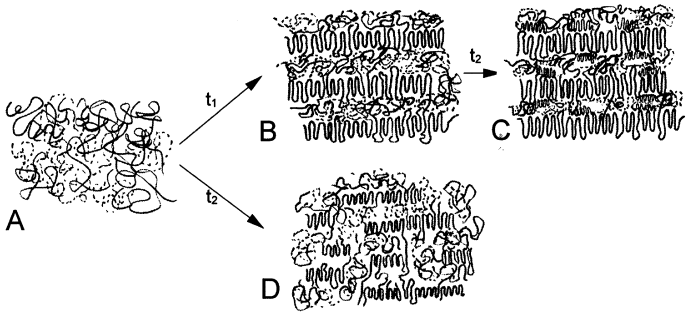

Fig. 15. Model describing the crystallization behavior of: (a) 80/20 PEO/Aramide blend; (b) after fast primary crystallization; (c) secondary crystallization; and a 65/35 PEO/Aramide blend after crystallization (d).

growth rate decreases strongly with increasing amount of amorphous component in the PEO/Aramide 34I blends. This results in the formation of less coarse lamellar folds and a higher value for the lamellar fold surface free energy. A change in the nucleation regime from II to III with increasing amount of Aramide 34I was illustrated. The changes in the crystallization behavior are related to the lower mobility of PEO in blends with Aramide, which in turn is related to the high T_g of Aramide 34I.

The melting behavior is complex and both the secondary crystallization and recrystallization can occur in the blends. At high amounts of PEO, a small fraction of PEO shows secondary crystallization forming low melting lamellae which, depending on the heating rate, can recrystallize during melting. In blends with larger amounts of Aramide 34I, only one type of lamellae is formed that can recrystallize during heating.

Both the supramolecular structure and the semi-crystalline morphology were investigated. The supramolecular structure changes from intermediate hedritic-spherulitic for pure PEO to spherulitic in blends above 15 wt.% Aramide. This change was attributed to the lower diffusion rate and increased secondary nucleation when crystallizing PEO in blends with Aramide 34I. During crystallization the amorphous component segregates between the lamellae, as indicated by the increase of both the long period and amorphous layer thickness. The lamellar insertion model in which thin lamellae are located between the primary formed thick lamellae in the same stack is proposed to describe the secondary crystallization of PEO in PEO/Aramide 34I blends.

Acknowledgements

This research was financially supported by the Research Council K.U. Leuven and the Fund for Scientific Research Flanders (FWO-Vlaanderen). One of the authors (G. Dreezen) is indebted to the Flemish Institute 'IWT' for a PhD research grant. We thank the European Union for support of the work at EMBL, Hamburg through the HCMP Access to Large Installations Project, Contract Number CHGE-CT93-0040.

References

[1] Tanaka H, Nishi T. Phys Rev Lett 1985;55(10):1102.
[2] Tanaka H, Nishi T. Phys Rev A 1989;39(2):783.
[3] Shibanov Y, Godovsky Y. Progr Colloid Polym Sci 1989;80:110.
[4] Li Y, Schneider L, Jungnickel B-J. Polym Net Blends 1992;2(3):135.
[5] Delimoy D, Goffaux B, Devaux J, Legras R. Polymer 1995;36(17):3255.
[6] Schulze K, Kressler J, Kammer H. Polymer 1993;34:3704.
[7] Cham PM, Lee TH, Marand H. Macromolecules 1994;27:4263.
[8] Inaba N, Yamada T, Suzuki S, Hashimoto T. Macromolecules 1988;21:407.
[9] Li Y, Jungnickel B-J. Polymer 1993;34:9.
[10] Wellscheid R, Wüst J, Jungnickel B-J. J Polym Sci B: Polym Phys 1996;34:267.
[11] Walsh D, Singh V. Makromol Chem 1984;185:1979.
[12] Guo W, Higgins JS. Polymer 1991;32:2115.
[13] Martuscelli E, Silvestre C, Gismondi C. Makromol Chem 1985;186:2161.
[14] Martuscelli E, Silvestre C, Addonizio ML, Amelino L. Makromol Chem 1986;187:1557.
[15] Silvestre C, Cimmino S, Martuscelli E, Karasz FE, Macknight WJ. Polymer 1987;28:1190.
[16] Silvestre C, Karasz FE, Macknight WJ, Martuscelli E. Eur Polym J 1987;23:745.
[17] Cimmino S, Martuscelli E, Silvestre C, Canetti M, de Lalla C, Seves A. J Polym Sci B: Polym Phys 1989;27:1781.
[18] Chow TS. Macromolecules 1990;23:333.
[19] Calahorra E, Cortazar M, Guzman GM. Polymer 1982;23:1322.
[20] Martuscelli E, Pracella M, Yue WP. Polymer 1984;25:1097.
[21] Pedrosa P, Pomposo JA, Calahorra E, Cortazar M. Polymer 1995;36:3889.
[22] Alfonso G, Russell T. Macromolecules 1986;19:1143.
[23] Silvestre C, Karasz FE, Macknight WJ, Martuscelli E. Eur Polym J 1987;23:745.
[24] Qin C, Pires A, Belfiore L. Polym Comm 1990;31:177.
[25] Kalfoglou N, Sotirpoulou D, Margaritas A. Eur Polym J 1988;24:389.
[26] Talibuddin S, Wu L, Runt J, Lin JS. Macromolecules 1996;29:7527.
[27] Nakata S, Kakimoto M, Imai Y. Polymer 1992;33:3873.
[28] Mathot VBF. In: Mathot VBF, editor. Calorimetry and thermal analysis of polymers, Hanser, 1994 chap. 5, p. 105–167; chap. 9, p. 231–299.
[29] Gaur U, Lau SF, Shu HC, Wunderlich BB. J Phys Chem Ref Data 1981;10:89 see also p. 119, 1001.

[30] Gaur U, Lau SF, Shu HC, Wunderlich BB. J Phys Chem Ref Data 1982;11:313 see also p. 1065.
[31] Gaur U, Lau SF, Shu HC, Wunderlich BB. J Phys Chem Ref Data 1983;12:29 see also p. 65, 91.
[32] Varma-Nair M, Wunderlich BB, Mehta A. J Phys Chem Ref Data 1991;20(2):349.
[33] Koch MHJ, Bordas J. Nucl Instrum Meth 1983;208:461.
[34] Boulin CJ, Kempf R, Gabriel A, Koch MHJ. Nucl Instrum Meth 1988;A269:312.
[35] Strobl G, Schneider MJ. J Polym Sci, Polym Phys Ed 1980;18:1343.
[36] Fox TG. Bull Am Phys Soc 1956;2:1123.
[37] Mandelkern L, Quinn FA, Flory PJ. J Appl Phys 1954;25:830.
[38] Hofmann JD, Davis GT, Lauritzen JI. In: Hannay NB, editor. Treatise on solid state chemistry, 3. New York: Plenum Press, 1976. p. 7 chap. 7.
[39] Turnbull D, Fischer JC. J Chem Phys 1949;17:71.
[40] Lauritzen JI, Hoffman JD. J Appl Phys 1973;44:4340.
[41] Paul DR, Barlow JW. Polymer alloys II, 11. New York: Plenum Press, 1980 p. 239.
[42] Arlie JP, Spegt P, Skoulios A. Makromol Chem 1967;104:212.
[43] Marentette JM, Brown GR. Polymer 1998;39:1415.
[44] Defieuw G, Groeninckx G, Reynaers H. Polymer 1989;30:2158.
[45] Defieuw G, Groeninckx G, Reynaers H. Polymer 1989;30:2164.
[46] Vanneste M, Groeninckx G. Polymer 1994;35:1051.
[47] Allen RC, Mandelkern L. J Polym Sci 1982;20:1465.
[48] Hoffman JD, Frolen LJ, Ross GS, Lauritzen JI. J Res Nat Bur Stand A Phys and Chem 1975;79A:671.
[49] Keith HD, Padden FJ. J Polym Sci; Polym Phys Ed 1987;25:229.
[50] Verma R, Marand H, Hsiao B. Macromolecules 1996;29:7767.
[51] Krüger K-N, Zachmann HG. Macromolecules 1993;26:5202.
[52] Hsiao B, Gardner KC, Wu D, Chu B. Polymer 1993;34:3986.